In-medium vector mesons and low mass lepton pairs from heavy ion collisions

Sourav Sarkar and Sabyasachi Ghosh

Theoretical Physics Division, Variable Energy Cyclotron Centre,
1/AF, Bidhannagar, Kolkata 700064, India

E-mail: sourav@vecc.gov.in

Abstract.

The ρ and ω meson self-energy at finite temperature and baryon density have been analysed for an exhaustive set of mesonic and baryonic loops in the real time formulation of thermal field theory. The large enhancement of spectral strength below the nominal ρ mass is seen to cause a substantial enhancement in dilepton pair yield in this mass region. The integrated yield after space-time evolution using relativistic hydrodynamics with quark gluon plasma in the initial state leads to a very good agreement with the experimental data from In-In collisions obtained by the NA60 collaboration.

1. Introduction

Colliding heavy ions at ultra-relativistic energies is the only way to produce and study bulk properties of strongly interacting matter. Systematic efforts, both theoretical and experimental over the last few decades [1, 2] have addressed various facets of the thermodynamics of the underlying theory − QCD. The spectra of hadrons emitted after freeze-out of the fireball produced in heavy ion collisions have provided us with a wealth of information. This includes the recent discovery made by studying the elliptic flow of hadrons that the quark gluon plasma (QGP) produced in Au+Au collisions at RHIC actually behaves as a strongly interacting fluid [3] as opposed to a asymptotically free gas of quarks and gluons. However, by virtue of the fact that electromagnetic probes (real photons and dileptons) are emitted all through the lifetime of the fireball coupled with their low rescattering probability make them penetrating probes capable of mapping the space-time history of the collision [4]. Lepton pairs with both invariant mass and transverse momentum information are in fact preferable to real photons. Large mass pairs produced by Drell-Yan process and from the decays of heavy quarkonia are emitted early whereas pairs with low invariant mass radiated from thermal hadronic matter and Dalitz decays of hadrons are produced late in the collision. The invariant mass spectra of dileptons thus carry time information as displayed explicitly in [5] using the invariant mass dependence of the elliptic flow of lepton pairs.

The rate of production of thermal dileptons is proportional to the two-point correlator of vector currents [6]. In the low invariant mass region which is dominated by lepton pairs produced during the later stages of the collision, dilepton emission takes place due to the decay of vector mesons. Consequently, the spectral properties of vector mesons, the ρ meson in particular has been a subject of intense discussion [7, 4, 2, 8]. We find that it is only for the $\pi - \pi$ loop that

one calculates the thermal self-energy loop for the vector mesons directly. In the case of other loops typically involving one heavy and one light particle or both heavy particles one uses in general either the virial formula or the Lindhard function.

The sources modifying the free propagation of a particle find a unified description in terms of contributions from the branch cuts of the self energy function. In addition to the unitary cut present already in vacuum, the thermal amplitude generates a new cut, the so called the Landau cut which provides the effect of collisions with the surrounding particles in the medium. This formalism was applied to obtain the ρ self-energy in hot mesonic [9] and baryonic [10] matter considering an exhaustive set of one-loop diagrams. The framework of real time thermal field theory that we use, enables us to evaluate the imaginary part of the self-energy from the branch cuts for real and positive values of energy and momentum without having to resort to analytic continuation as in the imaginary time approach. To evaluate the baryonic loops we work with the full relativistic baryon propagator in which baryons and anti-baryons manifestly appear on an equal footing. Thus the contributions from all the singularities in the self-energy function including the distant ones coming from the unitary cut of the loops involving heavy baryons are also included. These are not considered in the Lindhard function approach but can contribute appreciably to the real part of the ρ meson self-energy as shown [11] in the case of a $N\Delta$ loop.

The broadening of the vector meson spectral functions leads to an enhancement of lepton pair production in the invariant mass region below the ρ peak. The effect of the evolving matter is handled by relativistic hydrodynamics. The integrated yield is seen to agree very well with the NA60 data [12] from In-In collisions at 17.3 AGeV.

The article is organised as follows. We will begin with a short derivation of the the dilepton emission rate in terms of the current correlation function in section 2. The relation to the spectral function of vector mesons is specified in section 3. This will be followed by a discussion on ρ and ω self-energies in hot and dense matter in section 4. In section 5 a brief account of the space-time evolution and initial conditions will be provided followed by the dilepton invariant mass spectra. We will end with a summary in section 6.

2. Dilepton emission rate and the current correlation function

Let us consider an initial state $|I\rangle$ which goes to a final state $|F\rangle$ producing a lepton pair l^+l^- with momenta p_1 and p_2 respectively. The dilepton multiplicity thermally averaged over initial states is given by [13]

$$N = \sum_I \sum_F |\langle F, l^+l^-|e^{i\int \mathcal{L}_{int}d^4x}|I\rangle|^2 \frac{e^{-\beta E_I}}{Z} \frac{d^3p_1}{(2\pi)^3 2E_1} \frac{d^3p_2}{(2\pi)^3 2E_2} \tag{1}$$

where $Z = Tr[e^{-\beta H}]$ and $\mathcal{L}_{int} = e\overline{\psi}_l(x)\gamma_\mu\psi_l(x)A^\mu(x) + eJ^h_\mu(x)A^\mu(x)$ in which $\psi_l(x)$ is the lepton field operator and $J^h_\mu(x)$ is the electromagnetic current of hadrons. Following [6, 13, 4] this expression can be put in the form

$$\frac{dN}{d^4xd^4q} = \frac{e^4L(q^2)}{3(2\pi)^5q^4}e^{-\beta q_0}W^>_{\mu\nu}(q)(q^\mu q^\nu - q^2g^{\mu\nu}) \tag{2}$$

where, $W^>_{\mu\nu} = \int d^4x\ e^{iq\cdot x}\langle J^h_\mu(x)J^h_\nu(0)\rangle_\beta$ is the Fourier transform of the thermal expectation value of the two-point correlator of the hadronic currents and $L(q^2) = (1 + \frac{2m_l^2}{q^2})\sqrt{1 - \frac{4m_l^2}{q^2}}$. We now define $W^<_{\mu\nu}$ by interchanging the order of the currents getting $W^<_{\mu\nu} = e^{-\beta q_0}W^>_{\mu\nu}$. Using these to define the commutator $W_{\mu\nu} = W^>_{\mu\nu} - W^<_{\mu\nu} = \int d^4x\ e^{iq\cdot x}\langle[J^h_\mu(x), J^h_\nu(0)]\rangle_\beta$ we finally have

$$\frac{dN}{d^4xd^4q} = -\frac{\alpha^2}{6\pi^3}\frac{g^{\mu\nu}}{q^2}L(q^2)f_{BE}(q_0)W_{\mu\nu}(q_0, \vec{q}) \tag{3}$$

for conserved hadronic currents. This expression appears in different forms in the literature. Replacing $f_{BE}(q_0)W_{\mu\nu}$ in (3) by (i)$W^M_{\mu\nu} = \int d^4x\ e^{iq\cdot x}\langle J^h_\mu(x)J^h_\nu(0)\rangle_\beta$ yields the expression in [6], by (ii) $2\mathrm{Im}W^R_{\mu\nu}f_{BE}(q_0)$ where $W^R_{\mu\nu} = i\int d^4x\ e^{iq\cdot x}\theta(t-t')\langle[J^h_\mu(x), J^h_\nu(0)]\rangle_\beta$ yields the rate in [14] and by (iii) $2\mathrm{Im}W^T_{\mu\nu}/(1+e^{\beta q_0})$ where $W^T_{\mu\nu} = i\int d^4x\ e^{iq\cdot x}\langle T J^h_\mu(x)J^h_\nu(0)\rangle_\beta$ gives the rate in [15].

The rate given by eq. (3) is to leading order in electromagnetic interactions but exact to all orders in the strong coupling encoded in the current correlator $W_{\mu\nu}$. The q^2 in the denominator indicates the exchange of a single virtual photon and the Bose distribution implies the thermal weight of the source.

3. Current correlator and the spectral function of vector mesons

Thermal field theory is the appropriate framework to carry out perturbative calculations in the medium. In the real time version of this formalism two point functions assume a 2×2 matrix structure on account of the shape of the contour in the complex time plane [16, 17]. It is convenient to begin with the quantity,

$$T^{ab}_{\mu\nu} = i\int d^4x e^{iq\cdot x}\langle T_c J^h_\mu(x)J^h_\nu(0)\rangle_\beta \tag{4}$$

where T_c denotes ordering along the contour and a, b are the thermal indices which take values 1 and 2. This quantity can be diagonalised by means of a matrix U so that

$$T^{ab}_{\mu\nu} = U\begin{pmatrix} \overline{T}_{\mu\nu} & 0 \\ 0 & -\overline{T}^*_{\mu\nu}\end{pmatrix}U\ ; \quad U = \begin{pmatrix} \sqrt{1+n} & \sqrt{n} \\ \sqrt{n} & \sqrt{1+n}\end{pmatrix}\ , \quad n = \frac{1}{e^{\beta|q_0|}-1} \tag{5}$$

where $\overline{T}_{\mu\nu}$ is an analytic function. Equating both sides it follows that this function is obtainable from any one (thermal) component of $T^{ab}_{\mu\nu}$. It is related e.g. to the 11-component as,

$$\mathrm{Re}\overline{T}_{\mu\nu}(q_0,\vec{q}) = \mathrm{Re}T^{11}_{\mu\nu}(q_0,\vec{q})\ ;\ \ \mathrm{Im}\overline{T}_{\mu\nu}(q_0,\vec{q}) = \coth(\frac{\beta|q_0|}{2})\mathrm{Im}T^{11}_{\mu\nu}(q_0,\vec{q})\ . \tag{6}$$

Furthermore, $\overline{T}_{\mu\nu}$ has the spectral representation [18, 16]

$$\overline{T}_{\mu\nu}(q_0,\vec{q}) = \int\frac{dq'_0}{2\pi}\frac{W_{\mu\nu}(q'_0,\vec{q})}{q'_0 - q_0 - i\eta\epsilon(q_0)} \tag{7}$$

which immediately leads to

$$W_{\mu\nu}(q_0,\vec{q}) = 2\epsilon(q_0)\mathrm{Im}\overline{T}_{\mu\nu}(q_0,\vec{q})\ . \tag{8}$$

In the QGP where quarks and gluons are the relevant degrees of freedom, the time ordered correlation function $T^{11}_{\mu\nu}$ can be directly evaluated by writing the hadron current in terms of quarks of flavour f i.e. $J^h_\mu = \sum_f e_f\overline{\psi}_f\gamma_\mu\psi_f$. To leading order we obtain using relations (6) and (8),

$$g^{\mu\nu}W_{\mu\nu} = -\frac{3q^2}{2\pi}\sum_f e_f^2(1-\frac{4m_q^2}{q^2})\ . \tag{9}$$

The rate in this case corresponds to dilepton production due to process $q\overline{q}\to\gamma^*\to l^+l^-$. To obtain the rate of dilepton production from hadronic interactions it is convenient to break up the quark current J^h_μ into parts with definite isospin

$$\begin{aligned} J^h_\mu &= \frac{1}{2}(\bar{u}\gamma_\mu u - \bar{d}\gamma_\mu d) + \frac{1}{6}(\bar{u}\gamma_\mu u + \bar{d}\gamma_\mu d) + \cdots \\ &= J^V_\mu + J^S_\mu + \cdots \\ &= J^\rho_\mu + J^\omega_\mu/3 + \cdots \end{aligned} \tag{10}$$

where V and S denote iso-vector and iso-scalar currents and the dots denote currents comprising of quarks with strangeness and heavier flavours. These currents couple to individual hadrons as well as multiparticle states with the same quantum numbers and are usually labelled by the lightest meson in the corresponding channel [19]. We thus identify the isovector and isoscalar currents with the ρ and ω mesons respectively. Using eq. (10) in eq. (4) and neglecting possible mixing between the isospin states, we write

$$T^{ab}_{\mu\nu} = T^{(\rho)ab}_{\mu\nu} + T^{(\omega)ab}_{\mu\nu}/9 + \cdots \tag{11}$$

where

$$T^{(\rho)ab}_{\mu\nu} = i\int d^4x e^{iq\cdot x}\langle T_c J^\rho_\mu(x) J^\rho_\nu(0)\rangle_\beta \tag{12}$$

and similarly for the scalar current. The current commutator in the isospin basis follows as

$$W_{\mu\nu} = W^\rho_{\mu\nu} + W^\omega_{\mu\nu}/9 + ... \tag{13}$$

The correlator of vector-isovector currents $W^\rho_{\mu\nu}$ have in fact been measured [20] in vacuum along with the axial-vector correlator by studying τ decays into even and odd number of pions. The former is found to be dominated at lower energies by the prominent peak of the ρ meson followed by a continuum at high energies. The axial correlator, on the other hand, is characterised by the broad hump of the a_1. The distinctly different shape in the two spectral densities is an experimental signature of the fact that chiral symmetry of QCD is dynamically broken by the ground state [21]. It is expected that this symmetry may be restored at high temperature and/or density and will be signalled by a complete overlap of the vector and axial-vector correlators [22].

In the medium, both the pole and the continuum structure of the correlation function gets modified [4, 23]. We will first evaluate the modification of the pole part due to the self-energy of vector mesons in the following. Using Vector Meson Dominance the isovector and scalar currents are written in terms of dynamical field operators for the mesons allowing us to express the correlation function in terms of the exact(full) propagators of the vector mesons in the medium. Writing $J^\rho_\mu(x) = F_\rho m_\rho \rho_\mu(x)$ and $J^\omega_\mu(x) = 3F_\omega m_\omega \omega_\mu(x)$ in eq. (13) and using eq. (8) the current commutator becomes

$$W_{\mu\nu} = 2\epsilon(q_0)F^2_\rho m^2_\rho \mathrm{Im}\overline{D}^\rho_{\mu\nu} + 2\epsilon(q_0)F^2_\omega m^2_\omega \mathrm{Im}\overline{D}^\omega_{\mu\nu} + \cdots \tag{14}$$

where $\overline{D}_{\mu\nu}$ is the diagonal element of the thermal propagator matrix which is a two point function of the fields of vector mesons and is diagonalisable as in (5). The exact propagator is obtained in terms of the in-medium self-energies using the Dyson equation. Following [24] this is given by

$$\overline{D}_{\mu\nu}(q) = -\frac{P_{\mu\nu}}{q^2 - m^2_\rho - \overline{\Pi}_t(q)} - \frac{Q_{\mu\nu}/q^2}{q^2 - m^2_\rho - q^2\overline{\Pi}_l(q)} - \frac{q_\mu q_\nu}{q^2 m^2_\rho} \tag{15}$$

where $P_{\mu\nu}$ and $Q_{\mu\nu}$ are the transverse and longitudinal projections. The imaginary part is then put in eqs. (14) and then in eq. (3) to arrive at the dilepton emission rate [24]

$$\frac{dN}{d^4q d^4x} = \frac{\alpha^2}{\pi^3 q^2} L(q^2) f_{BE}(q_0)\left[F^2_\rho m^2_\rho A_\rho(q_0,\vec{q}) + F^2_\omega m^2_\omega A_\omega(q_0,\vec{q}) + \cdots\right] \tag{16}$$

where e.g. $A_\rho(= -g^{\mu\nu}\mathrm{Im}\overline{D}^\rho_{\mu\nu}/3)$ is given by

$$A_\rho = -\frac{1}{3}\left[\frac{2\sum \mathrm{Im}\Pi^R_t}{(q^2 - m^2_\rho - \sum \mathrm{Re}\Pi^R_t)^2 + (\sum \mathrm{Im}\Pi^R_t)^2} + \frac{q^2\sum \mathrm{Im}\Pi^R_l}{(q^2 - m^2_\rho - q^2\sum \mathrm{Re}\Pi^R_l)^2 + q^4(\sum \mathrm{Im}\Pi^R_l)^2}\right] \tag{17}$$

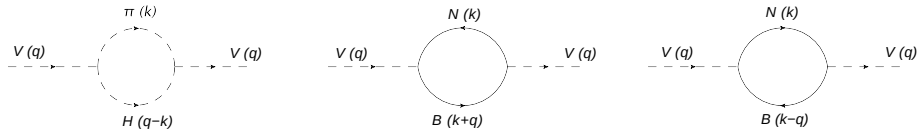

Figure 1. One-loop Feynman diagrams for ρ or ω self-energy involving mesons (first figure) and baryons (second and third figures). V stands for the ρ or ω in the external line. In the internal lines, h stands for π, ω, a_1 and h_1 mesons. For the baryonic loops, N and B indicate respectively nucleon and baryonic internal lines.

the sum running over all mesonic and baryonic loops. Thus, the dilepton emission rate in the present scenario actually boils down to the evaluation of the self energy graphs (shown in Fig. 1). The self-energy is also a 2×2 matrix and is diagonalisable by the matrix U^{-1}. The real and imaginary parts of the self energy function can then be obtained from the 11-component as [17, 10]

$$\begin{aligned} \mathrm{Re}\Pi^R_{\mu\nu}(q_0,\vec{q}) &= \mathrm{Re}\overline{\Pi}_{\mu\nu}(q_0,\vec{q}) = \mathrm{Re}\Pi^{11}_{\mu\nu}(q_0,\vec{q}) \\ \mathrm{Im}\Pi^R_{\mu\nu}(q_0,\vec{q}) &= \epsilon(q_0)\mathrm{Im}\overline{\Pi}_{\mu\nu}(q_0,\vec{q}) = \tanh(\beta q_0/2)\mathrm{Im}\Pi^{11}_{\mu\nu}(q_0,\vec{q}) \end{aligned} \tag{18}$$

where Π^R denotes the retarded self-energy.

As indicated earlier, coupling of the hadronic current to multiparticle states gives rise to a continuum structure in the current correlation function $W^{\mu\nu}$. Following Shuryak [19] we take a parametrised form for this contribution and augment the dilepton emission rate with

$$\frac{dN}{d^4q d^4x} = \frac{\alpha^2}{\pi^3} L(q^2) f_{BE}(q_0) \sum_{V=\rho,\omega} A_V^{\mathrm{cont}}. \tag{19}$$

where

$$A_\rho^{\mathrm{cont}} = \frac{1}{8\pi}\left(1+\frac{\alpha_s}{\pi}\right)\frac{1}{1+\exp(\omega_0-q_0)/\delta} \tag{20}$$

with $\omega_0 = 1.3, 1.1$ GeV for ρ, ω and $\delta = 0.2$ for both ρ and ω. The continuum contribution for the ω contains an additional factor of $\frac{1}{9}$.

4. Spectral function and self-energy of vector mesons

Obtaining the in-medium spectral functions for the ρ and ω mesons essentially involves the evaluation of the self-energies. For the ρ meson these have been evaluated recently for mesonic [9] and baryonic [10] loops. In the following we summarise these results for the ρ followed by those for the ω meson.

4.1. ρ meson

The 11-component of the self-energy of vector mesons for loops containing mesons or baryons can be generically expressed as

$$\Pi^{11}_{\mu\nu}(q) = i\int \frac{d^4k}{(2\pi)^4} L_{\mu\nu}(k,q)\Delta^{11}(k,m_k)\Delta^{11}(p,m_p)\ . \tag{21}$$

where the term $L_{\mu\nu}(k,q)$ contains factors from the numerators of the two propagators in the loop as well as from the two vertices and

$$\Delta^{11}(k,m_k) = \frac{-1}{k^2-m_k^2+i\epsilon} + a2\pi i\delta(k^2-m_k^2)N_1\ . \tag{22}$$

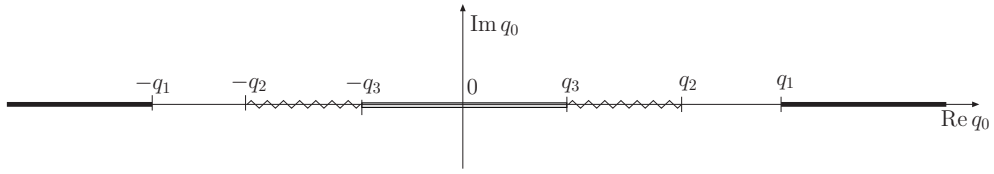

Figure 2. Branch cuts of self-energy function in q_0 plane for fixed $\vec{q}$ given by πh loop. The quantities $q_{1,2,3}$ denote the end points of cuts discussed in the text : $q_1 = \sqrt{(m_h + m_\pi)^2 + |\vec{q}|^2}$, $q_2 = \sqrt{(m_h - m_\pi)^2 + |\vec{q}|^2}$ and $q_3 = |\vec{q}|$.

For bosons, $a = 1$ and $N_1 = n$ with $n(\omega_k) = \frac{1}{e^{\beta\omega_k - 1}}$ whereas for fermions, $a = -1$ and $N_1 = n_+\theta(k_0) + n_-\theta(-k_0)$ with $n_\pm(\omega_k) = \frac{1}{e^{\beta(\omega_k \mp \mu)}+1}$. The loop momentum p in (21) for the various cases are as shown in Fig. (1).

We begin with mesonic loops. The ρ self-energy for four possible π-h loops, where $h = \pi, \omega, h_1, a_1$ have been evaluated. The imaginary part of the retarded self-energy (18) is given by,

$$\begin{aligned}
&\mathrm{Im}\Pi_R^{\mu\nu}(q_0, \vec{q}) = -\pi \int \frac{d^3\vec{k}}{(2\pi)^3 4\omega_\pi \omega_h} \times \\
&[L_1^{\mu\nu}\{(1 + n_\pi + n_h)\delta(q_0 - \omega_\pi - \omega_h) - (n_\pi - n_h)\delta(q_0 - \omega_\pi + \omega_h)\} \\
&+L_2^{\mu\nu}\{(n_\pi - n_h)\delta(q_0 + \omega_\pi - \omega_h) - (1 + n_\pi + n_h)\delta(q_0 + \omega_\pi + \omega_h)\}] \ . \qquad (23)
\end{aligned}$$

where the Bose distribution functions $n_\pi \equiv n(\omega_\pi)$ with $\omega_\pi = \sqrt{\vec{k}^2 + m_\pi^2}$ and $n_h \equiv n(\omega_h)$ with $\omega_h = \sqrt{(\vec{q} - \vec{k})^2 + m_h^2}$. $L_i^{\mu\nu}(i = 1, 2)$ are the values of $L^{\mu\nu}(k_0)$ for $k_0 = \omega_\pi, -\omega_\pi$ respectively and the vertices used in $L^{\mu\nu}(k_0)$ have been obtained from the chiral Lagrangians which are specified in [9].

The regions, in which the four terms of eq. (23) are non-vanishing, give rise to cuts in the self-energy function (Fig. 2). These regions are controlled by the respective δ-functions. Thus, the first and the fourth terms are non-vanishing for $q^2 \geq (m_h + m_\pi)^2$, giving the unitary cut, while the second and the third are non-vanishing for $q^2 \leq (m_h - m_\pi)^2$, giving the so-called Landau cut. The unitary cut arises from the states, which can communicate with the ρ. These states are, of course, the same as in vacuum, but, as we see above, the probabilities of their occurrence in the medium are modified by the distribution functions. On the other hand, the Landau cut appears only in medium and arises from scattering of ρ with particles present there. We note that this contribution appears as the first term in the virial expansion of the self-energy function.

Integrating over the angle and restricting to the kinematic region $q_0, q^2 > 0$ the contribution to the imaginary part coming from the unitary cut is given by [9]

$$\mathrm{Im}\Pi_R^{\mu\nu} = -\frac{1}{16\pi|\vec{q}|}\int_{\omega_\pi^-}^{\omega_\pi^+} d\omega_\pi L_1^{\mu\nu}\{1 + n(\omega_\pi) + n(q_0 - \omega_\pi)\} \qquad (24)$$

and that from the Landau cut is given by

$$\mathrm{Im}\Pi_R^{\mu\nu} = -\frac{1}{16\pi|\vec{q}|}\int_{\omega_\pi^{-\prime}}^{\omega_\pi^{+\prime}} d\omega_\pi L_2^{\mu\nu}\{n(\omega_\pi) - n(q_0 + \omega_\pi)\} \qquad (25)$$

where $\omega_{\pi\pm} = \frac{S_\pi^2}{2q^2}(q_0 \pm |\vec{q}|W_\pi)$, $\omega_{\pi\pm}{}' = \frac{S_\pi^2}{2q^2}(-q_0 \mp |\vec{q}|W_\pi)$ with $W_\pi = \sqrt{1 - \frac{4q^2 m_\pi^2}{S_\pi^4}}$ and $S_\pi^2 = q^2 - m_h^2 + m_\pi^2$.

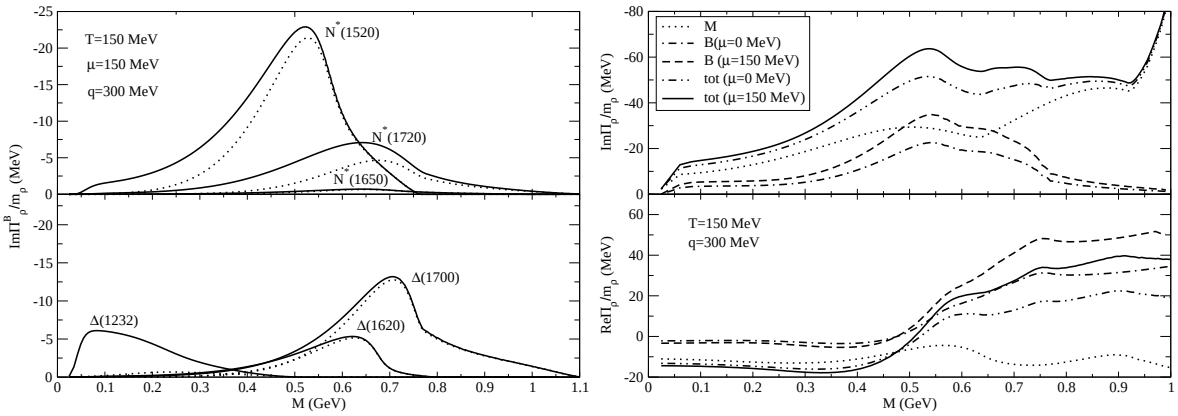

Figure 3. Left panel shows the imaginary part from baryonic loops and the right panel shows the total contribution from meson and baryon loops.

The real part can be obtained from the imaginary part by a dispersion relation or can be evaluated directly from the graphs.

Let us now turn to the baryonic loops in the ρ meson self-energy. Using $p = k - q$ for the third diagram of Fig. 1 in eq. (21) the retarded self-energy is evaluated for NB loops including all spin one-half and three-half 4−star resonances listed by the Particle Data Group so that B stands for the $N^*(1520)$, $N^*(1650)$, $N^*(1700)$, $N^*(1720)$ $\Delta(1230)$, $\Delta^*(1620)$, as well as the $N(940)$ itself.

As before, the imaginary part can be evaluated from the discontinuities of the self-energy. However, the threshold for the unitary cut for the baryon loops being far away from the ρ pole we only consider the Landau part. The expression of the self-energy corresponding to the second and third diagrams of Fig. 1 can be obtained from one another by inverting the sign of q. Adding the contributions coming from the two diagrams, the imaginary part of the self energy is given by

$$\mathrm{Im}\Pi_R^{\mu\nu} = -\frac{1}{16\pi|\vec{q}|}\int_{\omega_N^+}^{\omega_N^-} d\omega_N [L_1^{\mu\nu}(-q)\{n_+(q_0+\omega_N) - n_+(\omega_N)\} + L_2^{\mu\nu}(q)\{n_-(q_0+\omega_N) - n_-(\omega_N)\}] \tag{26}$$

where $\omega_N^{\pm} = \frac{S_N^2}{2q^2}(-q_0 \pm |\vec{q}|W_N)$ with $W_N = \sqrt{1 - \frac{4q^2m_N^2}{S_N^4}}$, $S_N^2 = q^2 - m_B^2 + m_N^2$. The factors $L_i^{\mu\nu}(i = 1, 2)$ in eq. (26) are the values of $L^{\mu\nu}(k_0)$ for $k_0 = \omega_N, -\omega_N$ respectively and is obtained using gauge invariant interactions details of which are provided in [10].

The calculations described above treats the heavy mesons and baryon resonances in the narrow width approximation. We have included their widths by folding with their vacuum spectral functions as done in [25].

We now present the results of numerical evaluation. We plot in the left panel of Fig. 3 the imaginary part of the ρ self-energy for baryon loops as a function of the invariant mass $\sqrt{q^2} \equiv M$ for $\vec{q} = 300$. The transverse (solid line) and longitudinal (dashed line) components $\mathrm{Im}\Pi_t$ and $q^2\mathrm{Im}\Pi_l$ have been shown separately. The $NN^*(1520)$ loop makes the most significant contribution followed by the $N^*(1720)$ and $\Delta(1700)$. On the right panel is plotted the spin-averaged ρ self-energy defined by $\Pi = \frac{1}{3}(2\Pi_t + q^2\Pi_l)$ showing contributions from the baryon and meson loops for two values of the baryonic chemical potential. The small positive contribution from the baryon loops to the real part is partly compensated by the negative contributions from the meson loops. The substantial baryon contribution at vanishing baryonic chemical potential reflects the importance of anti-baryons.

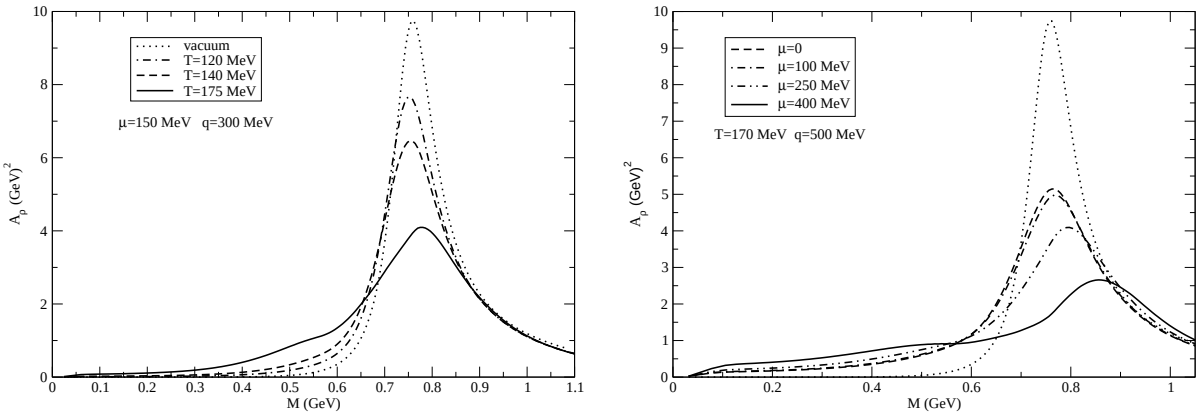

Figure 4. The spectral function of the ρ meson for (left) different values of the temperature T and (right) different values of the baryonic chemical potential (μ).

We now turn to the spin averaged spectral function defined in eq. (17). First, in the left panel of Fig.4 we plot the spectral function at fixed values of the baryonic chemical potential and three-momentum for various representative values of the temperature. We observe an increase of spectral strength at lower invariant masses resulting in broadening of the spectral function with increase in temperature. This is purely a Landau cut contribution from the baryonic loop arising from the scattering of the ρ from baryons in the medium. We then plot in the right panel of Fig. 4, the spectral function for various values of the baryonic chemical potential for a fixed temperature. For high values of μ we observe an almost flattened spectral density of the ρ.

4.2. ω meson

The ω self-energy is evaluated along similar lines [26]. The ω meson decays mostly into three pions. Assuming this decay to proceed via an intermediate ρ meson i.e. $\omega \to \rho\pi \to 3\pi$, the dominant contribution to the ω self-energy in meson matter can be expressed as [27]

$$\Pi^{\mu\nu}_{R(3\pi)}(q) = \frac{1}{N_\rho}\int_{4m_\pi^2}^{(q-m_\pi)^2} dM^2[\Pi^{\mu\nu}_{R(\pi\rho)}(q,M)]A_\rho(M) \tag{27}$$

where $N_\rho = \int_{4m_\pi^2}^{(q-m_\pi)^2} dM^2 A_\rho(M^2)$, A_ρ being the vacuum spectral function of the ρ. Here $\Pi^{\mu\nu}_{R(\pi\rho)}(q,M)$ can be obtained by evaluating the first diagram of Fig. (1) with $h=\rho$.

For ω self-energy due to baryons we have evaluated NB loops where $B = N^*(1440), N^*(1520), N^*(1535), N^*(1650), N^*(1720), N(940)$. The calculation proceeds similarly as in case of the ρ.

Left panel of Fig. (5) shows the transverse and longitudinal components of the imaginary part coming from the baryonic loops and the right panel shows the individual mesonic and baryonic loop contributions to the ω self-energy at two different chemical potentials. We see that the $N^*(1535)$ plays the dominating role mainly due to the strong coupling compared to the other baryonic resonances [27]. The spin averaged spectral function at different temperatures and chemical potentials are plotted in the left and right panels of Fig. (6) respectively. We observe a slight positive shift in the peak position.

Having obtained the in-medium spectral functions of the two most important low-lying vector mesons, we are now in a position to evaluate the static rate of dilepton production using eq. (16). Integrating over the transverse momentum q_T and rapidity y of the electron pairs we plot dR/dM^2 vs M in Fig. 7 for T=175 MeV. Because of the kinematical factors multiplying the ρ

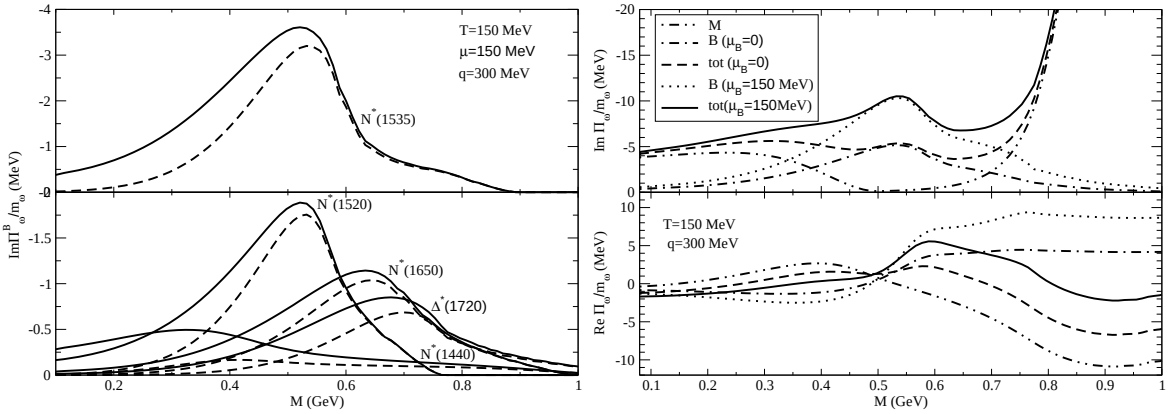

Figure 5. Same as Fig. (3) for the ω.

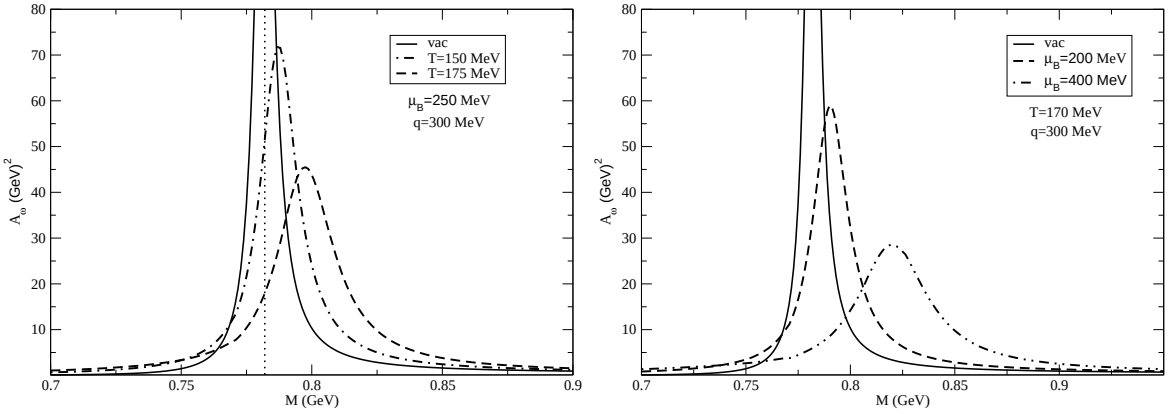

Figure 6. The spectral function of the ω for different values of T (left panel) and μ (right panel).

spectral function the broadening appears magnified in the dilepton emission rate. A significant enhancement is seen in the low mass lepton production rate due to baryonic loops over and above the mesonic ones shown by the dot-dashed line. The substantial contribution from baryonic loops even for vanishing chemical potential points to the important role played by antibaryons in thermal equilibrium in systems created at RHIC and LHC energies.

5. Space time evolution and dilepton spectra in In-In collisions

Since dileptons are produced at all stages of the collision it is necessary to integrate the emission rates over the space-time volume from creation to freeze-out. We assume that quark gluon plasma having a temperature T_i is produced at an initial time τ_i. Hydrodynamic expansion and cooling follows up to a temperature T_c where QGP undergoes a transition to hadronic matter. Subsequent cooling leads to freeze-out of the fluid element into observable hadrons. In the present work the fireball is taken to undergo an azimuthally symmetric transverse expansion along with a boost invariant longitudinal expansion [28]. The local temperature of the fluid element and the associated flow velocity as a function of the radial coordinate and proper time is obtained by solving the the energy momentum conservation equation $\partial_\mu T^{\mu\nu} = 0$ where $T^{\mu\nu} = (\epsilon + P)u^\mu u^\nu + g^{\mu\nu}P$ is the energy momentum tensor for ideal fluid. This set of equations are closed with the Equation of State (EoS); typically a functional relation between the pressure P and the energy density ϵ. It is a crucial input which essentially controls the profile of expansion

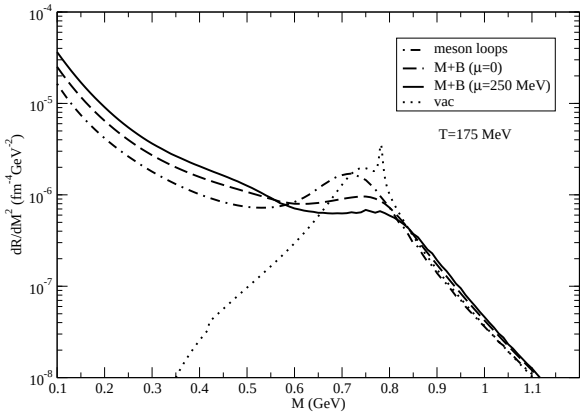

Figure 7. The lepton pair emission rate at $T = 175$ MeV with and without baryon (B) loops in addition to the meson (M) loops.

of the fireball.

The initial temperature is constrained by the experimentally measured hadron multiplicity through entropy conservation [29],

$$T_i^3(b_m)\tau_i = \frac{2\pi^4}{45\zeta(3)\pi\, R_\perp^2\, 4a_k}\langle\frac{dN}{dy}(b_m)\rangle \tag{28}$$

where $\langle dN/dy(b_m)\rangle$ is the hadron (predominantly pions) multiplicity for a given centrality class with maximum impact parameter b_m, $R_\perp$ is the transverse dimension of the system and a_k is the degeneracy of the system created. The initial radial velocity, $v_r(\tau_i, r)$ and energy density, $\epsilon(\tau_i, r)$ profiles are taken as [30], $v_r(\tau_i, r) = 0$ and $\epsilon(\tau_i, r) = \epsilon_0/(e^{\frac{r-R_A}{\delta}} + 1)$ where the surface thickness, $\delta = 0.5$ fm. In the present work we assume $T_c = 175$ MeV [31]. In a quark gluon plasma to hadronic matter transition scenario, we use the bag model EoS for the QGP phase and all resonances with mass ≤ 2.5 GeV for the hadronic gas. The transition region is parametrized as [32]

$$s = f(T)s_q + (1 - f(T))s_h \quad \text{with} \quad f(T) = \frac{1}{2}(1 + \tanh(\frac{T - T_c}{\Gamma}))\ . \tag{29}$$

where s_q (s_h) is the entropy density of the quark (hadronic) phase at T_c. The value of the parameter Γ can be varied to make the transition strong first order or continuous. We take $\Gamma = 20$ MeV in this work.

The ratios of various hadrons measured experimentally at different $\sqrt{s_{\rm NN}}$ indicate that the system formed in heavy ion collisions chemically decouple at a temperature ($T_{\rm ch}$) which is higher than the temperature for kinetic freeze-out (T_f)determined by the transverse spectra of hadrons [33]. Therefore, the system remains out of chemical equilibrium from $T_{\rm ch}$ to T_f. The chemical non-equilibration affects the dilepton yields through (a) the emission rate through the phase space factor and (b) the space-time evolution of the matter via the equation of state. The value of the chemical potential and its inclusion in the EoS has been taken into account following [34].

Finally, we have obtained the dimuon yield (dN/dM) in In-In collisions at SPS at a center of mass energy of 17.3 AGeV. The initial energy density is taken as 4.5 GeV/fm^3 corresponding to a thermalisation time $\tau_i = 0.7$ fm. We take the QGP to hadronic matter transition temperature $T_c = 175$ MeV and the freeze-out temperature T_f =120 MeV which can reproduce the slope of the hadronic spectra measured by the NA60 Collaboration. In Fig. (8) we have shown the

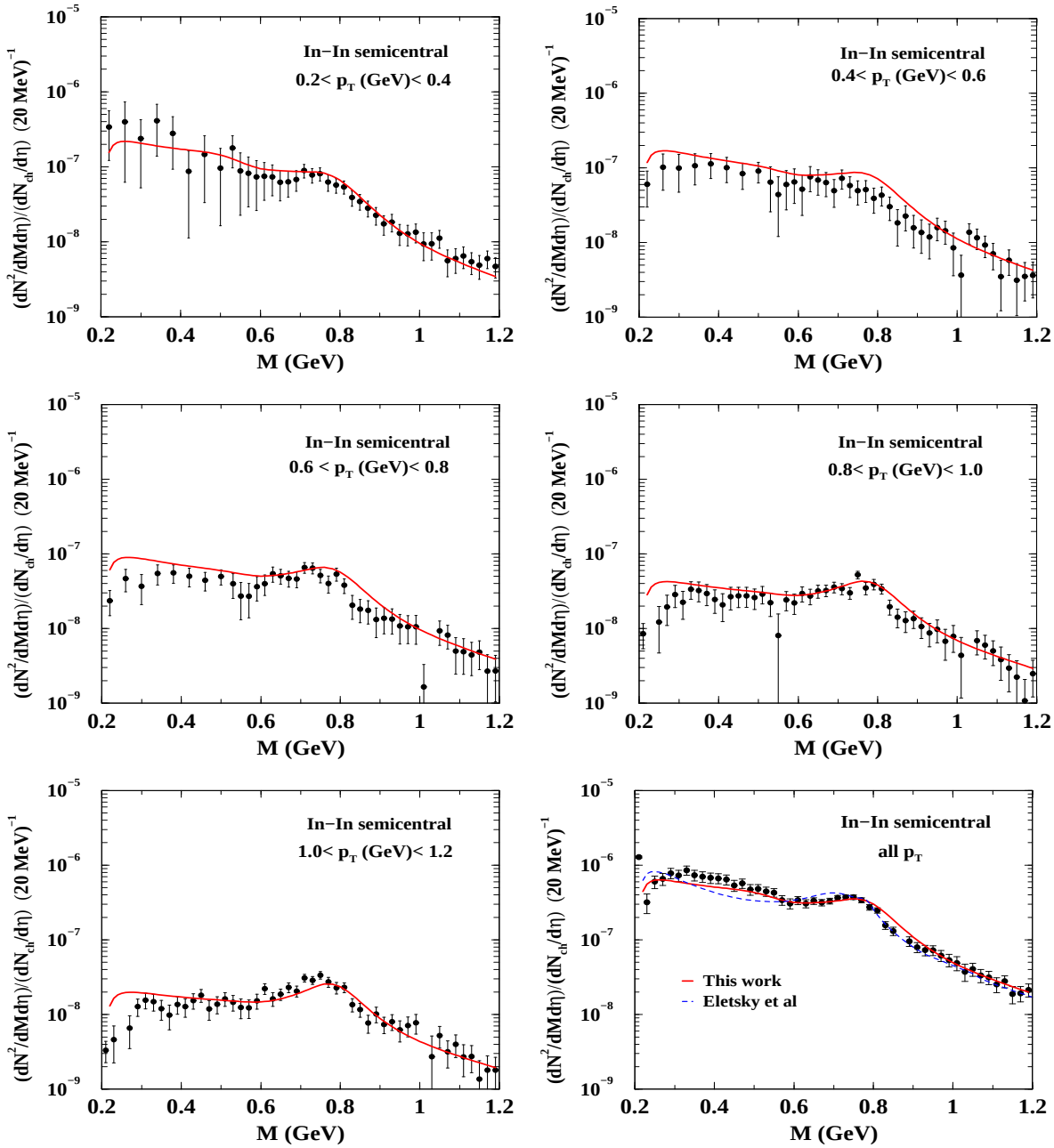

Figure 8. Dilepton invariant mass spectra for different p_T-bins compared with the NA60 data.

invariant mass spectra for different transverse momentum (p_T) windows. The theoretical curves agree quite well with the experimental data [12] for all the p_T ranges. The strong enhancement in the low M domain is clearly due to the large broadening of the ρ (and ω) in the thermal medium which comes entirely from the Landau cut in the self-energy diagrams. In the last panel we also plot for comparison the spectra calculated in [35] where the self-energy due to baryons has been evaluated following the approach of [36]. It is seen that this approach depicted by the dashed curve does not produce the required enhancement to explain the data in the range $0.35 \leq M \leq 0.65$ GeV.

6. Summary

The self-energy of ρ and ω mesons have been computed in nuclear matter at finite temperature and baryon density. Loop graphs involving mesons, nucleons and 4-star N^* and Δ resonances up to spin 3/2 were calculated using gauge invariant interactions in the framework of real time thermal field theory to obtain the correct relativistic expressions for the self-energy. The singularities in the complex energy plane were analysed and the imaginary part obtained from the Landau cut contribution. Results for the real and imaginary parts at non-zero three-momenta for various values of temperature and baryonic chemical potential were shown for the individual loop graphs. The spectral function of the ρ was observed to undergo a significant modification at and below the nominal rho mass which was seen to bring about a large enhancement of lepton pair yield in this region. After a space-time evolution using relativistic hydrodynamics, the invariant mass spectra for various p_T windows was found to be in very good agreement with the experimental data obtained in In-In collisions at 17.3 AGeV.

References

[1] "The Physics Of The Quark-Gluon Plasma," eds. S. Sarkar, H. Satz and B. Sinha, Lect. Notes Phys. **785**, 1 (2010).
[2] "The CBM Physics Book," eds. B. Friman et al, Lect. Notes Phys. **814**, 1 (2011).
[3] L. P. Csernai, J. I. Kapusta and L. D. McLerran, Phys. Rev. Lett. **97** (2006) 152303.
[4] J. Alam, S. Sarkar, P. Roy, T. Hatsuda, B. Sinha, Ann. Phys. 286, 159 (2000).
[5] P. Mohanty, V. Roy, S. Ghosh, S. K. Das, B. Mohanty, S. Sarkar, J. Alam and A. Chaudhuri, Phys. Rev. C **85** (2012) 031903.
[6] L. D. McLerran and T. Toimela, Phys. Rev. D **31**, 545 (1985).
[7] R. Rapp and J. Wambach, Adv. Nucl. Phys. **25**, 1 (2000)
[8] S. Leupold, V. Metag and U. Mosel, Int. J. Mod. Phys. E **19**, 147 (2010)
[9] S. Ghosh, S. Sarkar and S. Mallik, Eur. Phys. J. C **70**, 251 (2010)
[10] S. Ghosh and S. Sarkar, Nucl. Phys. **A 870-871**, 94 (2011)
[11] S. Ghosh, S. Sarkar and S. Mallik, Phys. Rev. C **83**, 018201 (2011).
[12] R. Arnaldi et al for the NA60 collaboration, Phys. Rev. Lett. **100** 022302 (2008); Eur. Phys. J. C **61**, 711 (2009); S. Damjanovic et al for the NA60 Collaboration, J. Phys. G: Nucl. Part. Phys. **35**, 104036 (2008).
[13] H. A. Weldon, Phys. Rev. D **42**, 2384 (1990).
[14] R. Rapp, J. Wambach and H. van Hees, arXiv:0901.3289 [hep-ph].
[15] J. V. Steele, H. Yamagishi and I. Zahed, Phys. Lett. B **384** (1996) 255.
[16] S. Mallik and S. Sarkar, Eur. Phys. J. C **61**, 489 (2009)
[17] M. Le Bellac, *Thermal Field Theory* (Cambridge University Press, Cambridge, 1996).
[18] S. Sarkar, B. K. Patra, V. J. Menon and S. Mallik, Indian J. Phys. **76A**, 385 (2002).
[19] E.V. Shuryak, Rev. Mod. Phys. 65, 1 (1993)
[20] R. Barate *et al.* [ALEPH Collaboration], Eur. Phys. J. C **4**, 409 (1998), K. Ackerstaff *et al.* [OPAL Collaboration], Eur. Phys. J. C **7**, 571 (1999)
[21] S. Sarkar, Nucl. Phys. A **862-863** (2011) 13.
[22] J. I. Kapusta and E. V. Shuryak, Phys. Rev. D **49**, 4694 (1994).
[23] S. Mallik and S. Sarkar, Eur. Phys. J. C **25**, 445 (2002).
[24] S. Ghosh, S. Sarkar, J. Alam Eur. Phys. J. C **71**, 9 (2011).
[25] S. Sarkar, E. Oset and M. J. Vicente Vacas, Nucl. Phys. A **750**, 294 (2005)
[26] S. Ghosh, S. Mitra and S. Sarkar, (under preparation)
[27] P. Muehlich, V. Shklyar, S. Leupold, U. Mosel, M. Post, Nucl. Phys. **A 780**, 187 (2006)
[28] J. D. Bjorken, Phys. Rev. D **27**, 140 (1983).
[29] R. C. Hwa and K. Kajantie, Phys. Rev. D **32**,1109 (1985).
[30] H. von Gersdorff, M. Kataja, L. D. McLerran and P. V. Ruskanen, Phys. Rev. D **34** 794(1986).
[31] S. Borsanyi *et al.*, Jour. High Eener. Phys. **1011**, 077 (2010).
[32] M. Asakawa and T. Hatsuda Phys. Rev. D **55** 4488 (1997).
[33] P. Braun-Munzinger, J. Stachel, J. P. Wessels and N. Xu, Phys. Lett. B **344** 43 (1995); **365** 1 (1996).
[34] T. Hirano and K. Tsuda, Phys. Rev. C **66** 054905 (2002).
[35] J. K. Nayak, J. e. Alam, T. Hirano, S. Sarkar and B. Sinha, arXiv:0902.0446 [nucl-th].
[36] V. L. Eletsky, M. Belkacem, P. J. Ellis and J. I. Kapusta, Phys. Rev. C **64** (2001) 035202

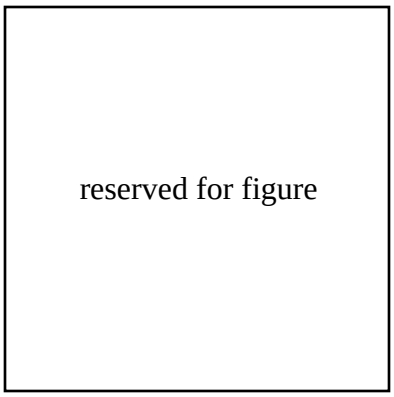
reserved for figure